OpenFOAM design sensitivity analysis on a homogeneous low-crested structure with concrete elements seaward of a vertical seawall to reduce overtopping

Jonker, R. G.; AlYousif, Ahmad; Hofland, B.; Antonini, Alessandro; Zoon, Arthur; Smith, Gregory

DOI
10.1016/j.oceaneng.2024.117423

Publication date
2024

Document Version
Final published version

Published in
Ocean Engineering

Citation (APA)
Jonker, R. G., AlYousif, A., Hofland, B., Antonini, A., Zoon, A., & Smith, G. (2024). OpenFOAM design sensitivity analysis on a homogeneous low-crested structure with concrete elements seaward of a vertical seawall to reduce overtopping. *Ocean Engineering*, *300*, Article 117423. https://doi.org/10.1016/j.oceaneng.2024.117423

Ocean Engineering 300 (2024) 117423

Contents lists available at ScienceDirect

Ocean Engineering

journal homepage: www.elsevier.com/locate/oceaneng

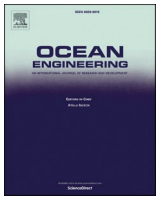

Research paper

OpenFOAM design sensitivity analysis on a homogeneous low-crested structure with concrete elements seaward of a vertical seawall to reduce overtopping

R.G. Jonker [a,c], Ahmad AlYousif [b,c,*], B. Hofland [c], Alessandro Antonini [c], Arthur Zoon [d], Gregory Smith [d]

[a] Aveco de Bondt, Nijkerk, Gelderland, the Netherlands
[b] Civil Engineering Department, Kuwait University, P.O. Box 5969, Safat, 13060, Kuwait
[c] Faculty of Civil Engineering and Geosciences, Delft University of Technology, Stevinweg 1, 2628 CN, Delft, the Netherlands
[d] Van Oord, Schaardijk 211, 3063 NH, Rotterdam, the Netherlands

ARTICLE INFO

Keywords:
Homogeneous low-crested structure
Cubipod concrete elements
CFD
OpenFOAM
Seawall overtopping
Wave transmission

ABSTRACT

This study treats a detached homogenous low-crested structure (HLCS) made of Cubipod concrete elements placed seaward of a vertical wall (forming a basin in between) to reduce overtopping. Assessing the complex hydrodynamics and effects of changing the geometry of such a system in relation to overtopping reduction is challenging. The numerical model OpenFOAM was applied to this end. Forchheimer coefficients for wave transmission and the flow through the HLCS were calibrated and validated using existing physical modeling data ($\alpha = 500$ and $\beta = 1.0$, with varying porosity based on the Cubipod shape), while the effect of the basin and vertical seawall was determined fully numerically. The crest freeboard (R_c), crest width (B), and basin length (L_B) were the main geometrical parameters that influenced the performance of the HLCS in reducing overtopping. An exponential decay was observed in the overtopping discharge when the values of these geometrical parameters increased. As L_B increased, this decay was primarily due to the dissipation of the broken-wave bores. The largest gradient in the predicted overtopping discharge was noted at $R_c/H_{s,i} \approx 0$, $B/H_{s,i} \approx 4.5$, and $L_B/L_p \approx 1.2$, where $H_{s,i}$ is the incident significant wave height and L_p is the peak wavelength in the basin.

1. Introduction

Seawalls are commonly used to protect coastal areas from flood risks and wave action, mainly because they occupy a limited space compared to other coastal protection structures (e.g., revetments). However, owing to climate change, an increase in sea level is expected in some parts of the world, which results in more overtopping discharges on coastal seawalls. Moreover, due to enhanced wave reflection, increased wave loads and moments are expected to act on vertical structures (AlYousif et al., 2021, 2022; Vijay et al., 2022a,b). Therefore, detached low-crested structures (LCS) are commonly used to reduce the direct wave attacks on seawalls (Roenby et al., 2017; Van den Bos and Verhagen, 2017). Sometimes, LCS (e.g., rubble-mound breakwaters or concrete reef-type elements) are used in combination with beach nourishment (Pilarczyk, 2003). Because the crest of the LCS is around the Still Water Level (SWL), it can be in emergent or submerged conditions, depending on the site's tidal range and the water level setup in a storm surge (Rock Manual, 2007). The LCS interacts with the incident waves, lowering their transmission on the lee side via wave reflection and energy dissipation. Detached LCS have several advantages over emerged structures, such as requiring fewer construction materials, allowing better water circulation, boosting the surrounding biodiversity, and enhancing the aesthetic appearance by reducing visual obstruction. These advantages encouraged the execution of a project called "Environmental Design of Low Crested Coastal Defense Structures" (DELOS) between 2001 and 2004. The objectives of this project were to analyze the hydrodynamics and stability of LCS, investigate their impact on biodiversity, quantify their benefits in different European countries, and develop operational guidelines for their design (Lamberti and Zanuttigh, 2004). Homogeneous low-crested structures (HLCS) are made of large armor rocks or precast concrete elements without a core. Concrete elements are typically used when stones of suitable quality are not

* Corresponding author. Civil Engineering Department, Kuwait University, P.O. Box 5969, Safat, 13060, Kuwait.
E-mail address: ahmad.alyousif@ku.edu.kw (A. AlYousif).

https://doi.org/10.1016/j.oceaneng.2024.117423
Received 30 October 2023; Received in revised form 5 March 2024; Accepted 6 March 2024
Available online 12 March 2024

available to protect the coast via conventional rubble mound LCS (Medina et al., 2019). These types of structures can protect the coastline in the same way as a conventional rubble mound LCS but have reduced environmental impact, a relatively clean construction phase, are easily adaptable, and fully reusable (Medina et al., 2019). Moreover, HLCS allow the passage of light through their porous concrete elements, which allows them to serve as green multipurpose reef structures (Odériz et al., 2018). Therefore, HLCS have multiple possible advantages over conventional rubble mound LCS depending on the local site conditions and availability of construction materials.

Most studies on wave transmission (Van der Meer, 1990; Van der Meer and Daemen, 1994; D'Angremond et al., 1996; Briganti et al., 2003; Van der Meer et al., 2005; Seabrook and Hall, 1998; Buccino and Calabrese, 2007) have been based on conventional rubble-mound LCS with a core and armor layer. However, the roughness values of the concrete elements, nominal median diameter (D_{n50}), and porosity of the HLCS were not similar. Structures with higher porosity, such as HLCS, are expected to exhibit different wave breaking at the crest compared to conventional rubble-mound LCS (Hattori and Sakai, 1994) and higher wave transmission (Buccino and Calabrese, 2007). Moreover, studies on water level setup prediction formulas (Longuet-Higgins, 1967; Diskin et al., 1970; Loveless et al., 1998; Calabrese et al., 2003) have been based on conventional rubble-mound LCS. Unlike conventional LCS, HLCS have a better capacity to restore the water level and lower the water level setup because of their higher permeability (Calabrese et al., 2008; Zanuttigh et al., 2008). Furthermore, HLCS are expected to experience less wave breaking owing to the shift in the incipient breaking location, which also lowers the wave-induced water level setup (Hattori and Sakai, 1994). Consequently, the hydrodynamic performance of the HLCS is different from that of the conventional rubble mound LCS. Therefore, the use of the prediction formulas developed for conventional rubble-mound LCS for HLCS is questionable. Molines et al. (2019) introduced an equation to predict wave transmission over a Cubipod HLCS that uses only the crest freeboard (R_c), which is the difference between the crest height (h_c) and water depth (h), as an input parameter. Hence, the effect of the HLCS on the water level setup behind the structure, as well as the effect of crest width (B) on wave transmission, are knowledge gaps and unknown. Wider crests are expected to have greater wave energy dissipation (D'Angremond et al., 1996) and continuous wave breaking along the crest, resulting in lower wave transmission. Furthermore, wider crests are expected to have more momentum release owing to waves breaking along the crest, and thus cause more water level setup within the basin. Increasing h_c for the submerged LCS is expected to increase the water level setup owing to the restricted return flow over the structure but decreases the wave transmission. The largest water level setup is expected for $R_c \approx 0$ (Loveless et al., 1998), whereas for emerged structures ($R_c > 0$), less water level setup is expected as less water overtops the crest of the structure.

It is a complex task to assess the hydrodynamics of a system consisting of a detached HLCS in front of a seawall to understand the effect of changing the geometrical layout of the HLCS on overtopping reduction at the seawall. From the literature review, it is noted that empirical prediction formulas for the overtopping discharge for the combination of a detached HLCS in front of a seawall are lacking. Moreover, the available prediction formulas for water level setup and wave transmission have either been developed for conventional rubble-mound LCS or lack the effect of the critical geometrical parameters of HLCS. Hence, it is necessary to optimize the design of such a system using numerical or physical modeling (or both). OpenFOAM is an advanced open-source CFD model based on Reynolds-averaged Navier (RANS) equations. To treat free-surface elevation, OpenFOAM uses the volume-of-fluid (VOF) method. If OpenFOAM is combined with the waves2Foam toolbox, it can be used to validate and model complex hydrodynamics in different types of coastal structures (Higuera et al., 2014a, 2014b; Jacobsen et al., 2015, 2017, 2018; Jensen et al., 2014; Molines et al., 2019). Unlike conventional breakwaters (e.g., rubble-mound breakwaters), OpenFOAM does not have validated porous media resistance parameters to be used for a structure consisting of a homogeneous layer of large concrete elements.

For the aforementioned knowledge gaps, the main objectives of this study are summarized as follows.

- To validate the porous media resistance parameters used for a HLCS (i.e., a reef-type structure) consisting of a homogeneous layer of large Cubipod concrete elements.
- Determine the influence of the main geometrical characteristics of a combined system of a detached HLCS in front of a seawall to reduce overtopping, and determine the dominant hydrodynamic phenomena.
- Provide design recommendations for these combined structures (i.e., HLCS in front of a seawall) to reduce overtopping.

The primary method used was detailed numerical modeling (using OpenFOAM). The elements of the HCLS are not resolved, but are modeled as a porous medium, of which the Forchheimer coefficients are calibrated using existing physical modeling data. The main geometrical parameters describing the combined HCLS-seawall structure were varied (h_c, B, and L_B). The value of the mean overtopping discharge (q) at the seawall is expected to be influenced by a combination of all hydrodynamics within the system (i.e., wave transmission, water level setup, and seiching-resonance). The larger basin lengths, which are the distances between the HLCS and the seawall, are expected to have a lower water level setup because of the available storage volume inside the basin, depending on the restoring abilities of the HLCS. Increasing the crest width or height is expected to reduce the overtopping discharge due to the reduction in wave transmission. For basin lengths equal to the seiching-resonance frequency of the basin, more overtopping discharge is expected.

The scope of this study is limited to a cross-shore two-dimensional configuration, with long-crested waves and a basin between the HCLS and seawall that is closed off from the sides, thus hindering the outflow of water to the sides. A single hydraulic boundary condition was used in the parametric study as listed in Table 1.

The remainder of this paper is organized as follows: Section 2 describes the physical modeling experiment, numerical model, and calibration and validation processes. Section 3 discusses the results of the design sensitivity analysis, use of OpenFOAM to model the effect of the HLCS on wave transmission, and design recommendations. Section 4 presents the main conclusions and directions for future studies.

2. Methodology

2.1. The geometry of available test data

The numerical model setup used in this study was based on a two-dimensional no-damage physical modeling experiment performed by Medina et al. (2019) and Odériz et al. (2018) with a length scale of 1:37.5. To calibrate and validate the OpenFOAM model, an experiment was conducted on five layers of the Cubipod HLCS under irregular waves. In this experiment, the HLCS has B of 0.11 m, h_c of 0.23 m, and the structure's base width (W) of 0.59 m. Moreover, to calibrate the OpenFOAM model, the experimental data of observed wave transmission coefficients (K_t) by Medina et al. (2019) were used. Hence, the transmitted significant ($H_{s,t}$) and incident significant ($H_{s,i}$) wave heights were measured, and K_t was calculated as follows:

$$K_t = H_{s,t}/H_{s,i}.. \quad (1)$$

The HLCS was installed on a flat platform, elevated by 0.1 m, and has a foreshore slope of 0.02. Experiments were performed with a sampling rate of 100 Hz for H_s and R_c values in the range of 4.5–11.6 cm and −1.0-4.0 cm, respectively. The Cubipod units had a mass density (ρ_c) of 2280 kg/m^3, D_{n50} of 4.35 cm, and were placed in a triangular grid

Table 1
Applied system characteristics and boundary conditions to the OpenFOAM model for the basic configuration of the parametric study. For more in-depth details on the boundary conditions on all performed simulations, the reader is referred to Jonker (2020).

	Input	Symbol	Value	Unit
Hydraulic	The spectral		JONSWAP	
	The factor of peak enhancement	γ	3.3	[-]
	Offshore water depth at WG00	h_0	33	[cm]
	Water depth in the basin at WG05	h	23	[cm]
	Incoming measured significant wave height at WG02	$H_{s,i}$	11.24	[cm]
	Incoming measured peak period	$T_{p,i}$	1.63	[s]
	Incoming measured peak wavelength	L_p	230	[cm]
	Number of waves	N	500	[-]
Geometrical Parameters	HLCS Structure height	h_c	23	[cm]
	HLCS Crest freeboard	R_c	0	[cm]
	HLCS Crest width	B	33	[cm]
	HLCS Base width	W	59	[cm]
	Basin length	L_B	277	[cm]
	Seawall Crest freeboard	$R_{c,seawall}$	6	[cm]
HLCS numerical	Alpha	α	500	[-]
	Beta	β	1.0	[-]
	Core porosity	$n_{p,core}$	50	[%]
	Outer layer porosity	$n_{p,outer}$	75.2	[%]
	Keulegan-Carpenter number	KC	13.15	[-]
	Nominal diameter	D_{n50}	4.35	[cm]
Seawall numerical	Front face Openness	e_p	3	[%]
	Front face Head loss coefficient	ξ_p	1.5	[-]
System	Simulation duration		680	[s]
	Solver		InterFOAM	[-]

configuration.

2.2. Numerical model description

The numerical framework used in this research is called CoastalFOAM, which contains various packages of OpenFOAM (e.g., waves2Foam, coupling to OceanWave3D, and permeable interactions) that can be used to model complex wave-structure interactions and coastal zone environments. Moreover, non-open-source tools and processing utilities were implemented in the numerical framework. These additions were developed as part of the JIP CoastalFOAM Program, founded by the following engineering companies: Royal Haskoning DHV, Boskalis Westminster, Van Oord, and Deltares. Using OpenFOAM combined with the waves2Foam toolbox to model the hydrodynamics of permeable structures has been implemented and validated in several studies (Jacobsen et al., 2015, 2017, 2018; Jensen et al., 2014). A similar implementation was made by Higuera et al. (2014a,b) for IHFOAM. In this study, the relaxation zone techniques described by Paulsen et al. (2014) were used to couple OpenFOAM and the efficient potential flow solver OceanWave3D in the waves2Foam toolbox, such that the OpenFOAM domain was nested within a larger OceanWave3D domain. Further details of the numerical model set-up are provided in the next section. For more information on OceanWave3D, please refer to Engsig-Karup et al. (2009).

In OpenFOAM, RANS equations are used to compute the hydrodynamics of the flow velocities and pressures for a two-phase flow. For coastal engineers, a macroscopic approach for obtaining the flow through a permeable material is more applicable because of the relatively large size of the structures (Losada et al., 2016). This approach has been validated for different coastal structures (Jacobsen et al., 2015; Van Gent, 1995) as presented by Jensen et al. (2014), in which the equations of the volume-averaged RANS (VARANS) are described as

$$\left(1+c_p\right)\frac{\partial}{\partial t}\frac{\rho \boldsymbol{u}}{n_p}+\frac{1}{n_p}\nabla\frac{\rho}{n_p}\boldsymbol{u}\boldsymbol{u}^T=-\nabla p^*+\boldsymbol{g}\bullet\boldsymbol{x}\nabla\rho+\frac{1}{n_p}\nabla\bullet\mu\nabla\boldsymbol{u}-\boldsymbol{F}_p;\nabla\bullet\boldsymbol{u}=0, \tag{2}$$

where c_p is the added mass coefficient, t is time, ρ is the fluid density, $\boldsymbol{u}$ is the filter velocity in Cartesian coordinates, $\boldsymbol{u}^T$ is the transpose of $\boldsymbol{u}$, n_p is the porosity, $\nabla=\left(\frac{\partial}{\partial x},\frac{\partial}{\partial y},\frac{\partial}{\partial z}\right)$ is the gradient operator, $p^*=p-\rho\boldsymbol{g}\boldsymbol{x}$ is the excess pressure, p is the total pressure, $\boldsymbol{g}$ is the vector of gravitational acceleration, $\boldsymbol{x}=(x,y,z)$ is the Cartesian coordinate vector, μ is the dynamic viscosity, and $\boldsymbol{F}_p$ is the vector of flow resistance due to the interaction with the porous structure. The coefficient c_p in Eq. (2) was calculated as given by Van Gent (1995).

$$c_p=\gamma_p\frac{1-n_p}{n_p}, \tag{3}$$

where γ_p is an empirical coefficient that is usually set as 0.34 (Van Gent, 1995; Jensen et al., 2014) and the $\boldsymbol{F}_p$ is calculated as adopted in the momentum equation as:

$$F_p=a_p\rho\boldsymbol{u}+b_b\rho\|\boldsymbol{u}\|_2\boldsymbol{u}, \tag{4}$$

where a_p and b_b are the drag force-resistance coefficients. These two coefficients are calculated according to Van Gent (1995) as follows:

$$a_p=\alpha\frac{\left(1-n_p\right)^2}{n_p^3}\bullet\frac{\mu}{\rho D_{n50}^2} \tag{5}$$

and

$$b_p=\beta\left(1+\frac{7.5}{KC}\right)\bullet\frac{1-n_p}{n_p^3}\frac{1}{D_{n50}}, \tag{6}$$

Where α and β are the closure coefficients and KC is the Keulegan-Carpenter number, which is at the toe of the structure as defined by Jacobsen et al. (2015):

$$KC=\frac{H_{m_0}}{2}\sqrt{\frac{g}{h}}\frac{1.1\ T_{m-1,0}}{D_{n50}}, \tag{7}$$

The magnitude of the closure coefficients (α and β) are strongly influenced by the flow regime, which can be identified by obtaining the pore Reynolds number (Re_p) as (Jensen et al., 2014):

$$Re_p=\frac{\langle\overline{u}\rangle\ D_{n50}}{n_p\nu}, \tag{8}$$

where $\langle\overline{u}\rangle$ the average flow velocity per time step per control volume (computational cell) and ν is the kinematic viscosity. For concrete elements, Re_p value is in the order of $1x10^5$ (Jensen et al., 2014), which is a fully turbulent flow regime with a dominance of the β coefficient (Jensen et al., 2014; Losada et al., 2016).

A large range of values has been reported in the literature for closure coefficients, and no predictive methodology has been developed. Hence, as noted by del Jesus et al. (2012), calibration was required. Jensen et al. (2014) and Jacobsen et al. (2015) showed the possibility of correctly representing bulk hydrodynamics (i.e., free-surface elevation, wave absorption, and wave reflection) without directly accounting for turbulence. The amount of turbulence depends on the dimensions of the elements of the HLCS, magnitude of the incoming waves, and dimensions of the HLCS. Hence, turbulence is produced inside the HLCS. The turbulence inside the porous media is integrated within the closure coefficients (α and β) and KC, as Jensen et al. (2014) suggested. No

additional turbulence models were adopted outside the porous media. OpenFOAM uses the VOF method to solve two-phase free-surface Newtonian fluids and tracks the highly nonlinear interface between the fluids (water and air), as introduced by Jensen et al. (2014).

$$\frac{\delta F}{\delta t}+\frac{1}{n_p}[\nabla \bullet \boldsymbol{u}F+\nabla \bullet \boldsymbol{u}_r(1-F)F]=0, \tag{9}$$

where F is the indicator field function, which is the volume ratio of water to air per computational cell, $\frac{1}{n_p}$ is a factor included by Jensen et al. (2014) to ensure the conservation of mass for the fluid motion through the porous structure, and $\boldsymbol{u}_r$ is the relative velocity, which compresses the solution at the interface (for more details on $\boldsymbol{u}_r$, please refer to Berberović et al. (2009)). OpenFOAM uses wave relaxation zones to generate and absorb free-surface water waves via the waves2Foam toolbox (Jacobsen et al., 2012). The value of q (m^3/s) at each time step in a structure was measured using the waves2Foam toolbox by defining an overtopping face (Jacobsen et al., 2017). When $F = 1$, it is assumed that the fluid is water, and q over a set of faces (f) can be estimated as (Jacobsen et al., 2017):

$$q=\sum_{f\in \mathrm{f}}\varphi_{F,f}\frac{\boldsymbol{s}_f}{\|\boldsymbol{s}_f\|_2}, \tag{10}$$

where $\boldsymbol{s}_f$ is the non-unit normal vector to the face and φ_F is the flux of fluid across a face multiplied by the indicator function field F.

2.3. Numerical model setup

In this study, different numerical model setups were used within the same numerical wave flume as follows.

- The first configuration, which did not include the HLCS or seawall, was used to verify the hydrodynamic wave flume.
- The second configuration did not include the HLCS but included the seawall and was used to verify the overtopping behavior by comparing the model overtopping results with the EurOtop prediction formula.
- The third configuration was based on physical model experiments conducted with the HLCS but without the seawall, and was used to calibrate and validate the hydrodynamic behavior of the HLCS.
- The fourth configuration is the basic configuration, which includes the HLCS and seawall, as shown in Fig. 1, and uses the same hydraulic boundary conditions as in the third configuration. The final configuration was used for the parametric study by changing the geometrical layout of the system. If necessary, a fictitious length scale 37.5 is used to report the results on a realistic scale.

The numerical wave flume had a length and height of 25.08 m and 0.59 m, respectively. As in the physical modeling experiment, a platform that starts at $x = 6.58$ m with a forehead slope and height of 0.02 and 0.1 m was used. The numerical flume consists of a nested OpenFOAM model within a larger Oceanwave3D model, as presented in Fig. 1. At $x = 0$ m, waves were generated, and at $x = 5$ m, information on the free-surface elevation was coupled from OceanWave3D to the OpenFOAM domain. The waves within OpenFOAM were absorbed using the outlet relaxation zone, and at $x = 21$ m, the waves within OceanWaves3D were absorbed using the outlet relaxation zone based on pressure damping. To obtain wave data from the numerical flume, nine wave gauges were placed at the exact locations used in the physical modeling experiment, as shown in Fig. 1. For the parametric study, additional 81 wave gauges were installed with increments of 0.1 m starting at $x = 17$ m. Rectangular grid cells were used over the complete numerical domain using block-MeSH. It is recommended to use orthogonal grid cells to obtain an aspect ratio of 1 ($\Delta x = \Delta y$), where the free surface is expected as it has a substantial impact on the wave propagation performance of OpenFOAM (ITTC, 2011; Jacobsen et al., 2012; Roenby et al., 2017). This resulted in a grid size of $\Delta x = \Delta y$ of 0.011 m (10 grid cells per significant wave height). Furthermore, refinements (1/4 of the original size) were applied at the regions of interest (near the free surface, HLCS, and seawall) using snappyHexMesh. A maximum Courant number (C_{max}) of 0.2 is used.

The hydraulic boundary conditions used to calibrate the wave flume hydrodynamics and the parametric study are presented in Table 1. The conditions were selected such that these hydraulic boundary conditions without HLCS cause severe overtopping at a prototype scale of 294 l/s/m, which corresponds to structural damage at a non-paved revetment seawall (Rock Manual, 2007). Furthermore, the usage of these relatively large hydraulic boundary conditions enhances the quality of comparison in the overtopping discharges while maintaining the stability of the HLCS elements (i.e., $\frac{H_s}{\Delta D} \approx 2$). Moreover, the wave height is such that realistic wave breaking conditions occur on the sloping foreshore, as often is the case in design. The applied offshore boundary wave height (H_s) resulted in a measured incoming significant wave height at gauge WG02 ($H_{s,i}$) of 11.24 cm due to wave shoaling with a measured peak wave period ($T_{p,i}$) and wavelength (L_p) of 1.63 s and 230 cm, respectively.

The third configuration was used to calibrate and validate the porous media coefficients for the HLCS. No additional turbulence model is included as all the turbulence effects are calibrated in the calibrated porous media resistance coefficients (α and β). For the basic configuration and parametric study, the fourth model configuration consisted of a seawall installed on the lee side of the HLCS, where an overtopping face was applied on the top and front sides of the structure to measure the overtopping discharges and wave forces, respectively. An openness and head loss coefficients of 3% and 1.5, respectively, were adopted, which Jacobsen et al. (2018) validated for the force prediction of a crown wall installed on a rubble-mound breakwater. In all the simulations, 500 waves were used, following the recommendations of Romano et al. (2015) for overtopping simulations.

2.4. Numerical model calibration and validation procedure

The calibration and validation procedures are ideally based on raw water surface elevation data, overtopping volumes, pressures, or steering paddle input signals. However, because these data were unavailable

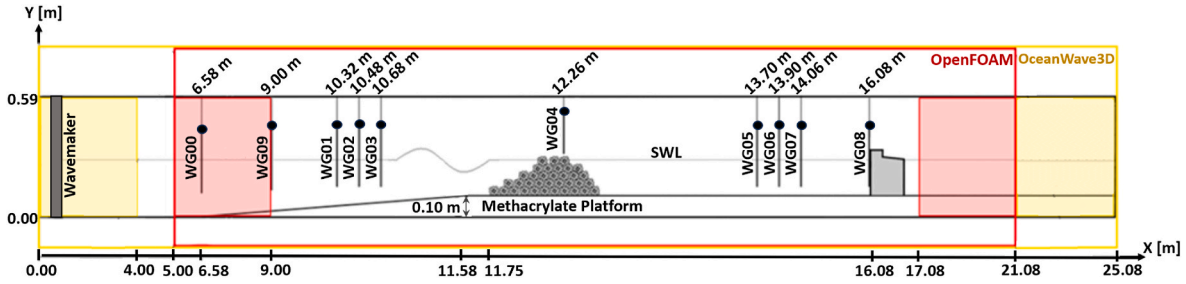

Fig. 1. Layout of the numerical flume that includes the OceanWave3D and OpenFOAM domains as used for the parametric study (not to scale). For the calibration of the HLCS, there was no seawall implemented.

to the authors, a general approach was adopted.

2.4.1. Verification of wave flume hydrodynamics

OpenFOAM has been proven to be fully capable of describing irregular wave fields, overtopping, and porous flow through structures (Jacobsen et al., 2012, 2015; Jensen et al., 2014). In this study, a comparable grid resolution (10 grid cells per wavelength), grid shape (rectangular with an aspect ratio of 1), Courant number ($C_{max} = 0.2$), and coupling techniques with relaxation zones (minimum of one wavelength long) were applied. However, to verify the implementation of the model configuration, the bulk wave flume hydrodynamics (surface-level elevation and overtopping) were verified. The verification process consisted of the following three steps:

- Step 1: Numerical flume configuration-1 without the HLCS and seawall. An analysis was performed on the direct coupling between both models (OpenFOAM and OceanWave3D) on raw surface elevation signals at the coupling zone for different grid resolutions and Courant numbers using the Pearson Correlation Coefficient (PCC) and root mean squared error (RMSE) to determine the goodness of fit.
- Step 2: Numerical flume configuration-1 without the HLCS and seawall. The wave propagation was analyzed after reaching the coupling zone. This was achieved by comparing the water surface elevation signals and statistical parameters between the output of the standalone OceanWave3D model and those of the coupled OpenFOAM and OceanWave3D models. for different grid resolutions and number of courts. For the adopted model setup, the difference between the computed statistical wave parameters of the OpenFOAM and OceanWave3D outputs is approximately 1%. For further details on the verification procedure, refer to Jonker et al.(2020).
- Step 3: Numerical flume configuration-2 without the HLCS but with the seawall. For different freeboard values of the seawall ($R_{c,seawall}$), the adapted grid resolution and Courant number from the previous step were compared to the CLASH database and EurOtop 2018 design guidelines for impulsive overtopping conditions, which were calculated for $0 < R_{c,seawall}/H_{m_0} < 1.35$ as (Van der Meer et al., 2018):

$$\frac{q}{\sqrt{gH_{m_0}^3}} = 0.011\left(\frac{H_{m_0}}{h\, s_{m-1,0}}\right)^{0.5}\left(e^{-2.2\frac{R_{c,seawall}}{H_{m_0}}}\right), \tag{11}$$

where $s_{m-1,0}$ is the wave steepness. For $R_{c,seawall}/H_{m_0} \geq 1.35$, the overtopping discharge is calculated as (Van der Meer et al., 2018):

$$\frac{q}{\sqrt{gH_{m_0}^3}} = 0.0014\left(\frac{H_{m_0}}{h\, s_{m-1,0}}\right)^{0.5}\left(\frac{R_{c,seawall}}{H_{m_0}}\right)^{-3}.. \tag{12}$$

To obtain the reflected waves from the incoming signal, a wave-reflection procedure based on Zelt and Skjelbreia (1993) was used. A high agreement is observed in Fig. 2 between the predicted mean overtopping discharge by OpenFOAM and both the EurOtop formulas and CLASH database.

2.4.2. Calibration and validation of HLCS hydrodynamic behavior

Water flowing through the HLCS experiences resistance, which causes energy dissipation. As described in section 2.2 (Eqs. (5) and (6)), the flow resistance is influenced by D_{n50}, KC, n_p, as well as the closure coefficients α and β. Calibration was performed on α and β using the third numerical model configuration corresponding to the physical model experiments. In addition, considerable effort has been devoted to correctly defining the layered porosity of HLCS using large concrete elements.

In this study, the values of D_{n50}, KC, and n_p were kept constant in the numerical model. Using Eq. (7), KC was obtained as 13.15, indicating that the flow was turbulent with a related vortex shedding and drag force. The D_{n50} has a constant value based on the physical model experiments of 4.35 cm.

2.4.2.1. HLCS porosity. Volume-averaged numerical models typically consider a homogeneous value for porosity within computational cells; thus, they lack knowledge of the boundary effect. However, this can influence wave breaking in the structure. Although HLCS consist of a single type of large concrete element without a core, two numerical layers were implemented in OpenFOAM to have a good numerical representation of the higher porosity of the structure in the outer boundary layer. A study was conducted on the porosity distribution of the Cubipod concrete elements to determine the thickness and porosity of the numerical outer layer. For the numerical core layer, the measured porosity of the HLCS in the physical model experiments is used, which is 50%.

We derived the solidity curve distribution for each randomly placed Cubipod orientation. Nine different orientations were obtained that described all possible orientations within 22.5° increments. The sample solidity curve distribution for one of the nine orientations in 22.5° increments is shown in Fig. 3. As expected, large solidity gradients over the vertical distance were observed for all the orientations, particularly near the boundaries. The porosity distribution for each orientation was obtained as porosity = 1 − solidity. The porosity profile presented in Fig. 4 is the mean of the porosity distributions for all nine orientations.

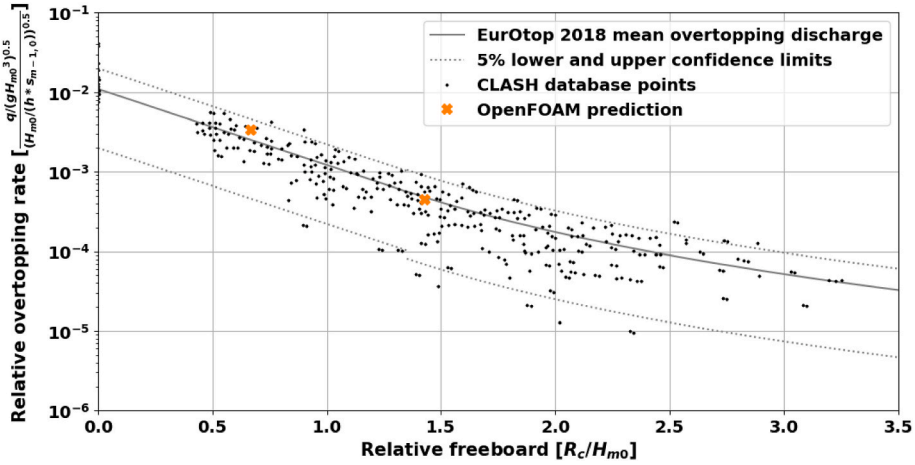

Fig. 2. Comparison between the CLASH database, EurOtop 2018 empirical prediction formulas, and OpenFOAM predictions for the mean overtopping discharge for the seawall with different freeboards. Data are obtained from Van der Meer et al. (2018).

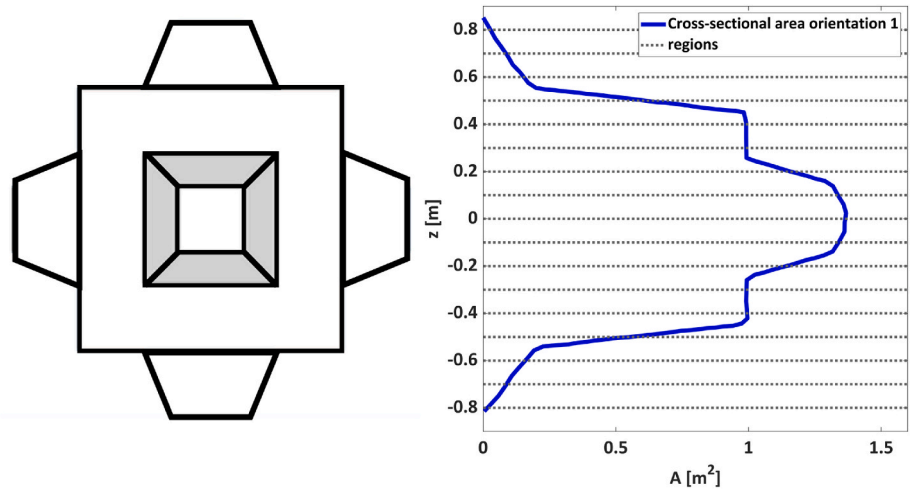

Fig. 3. Sample solidity curve distribution for one of the Cubipod orientations with 22.5° increments.

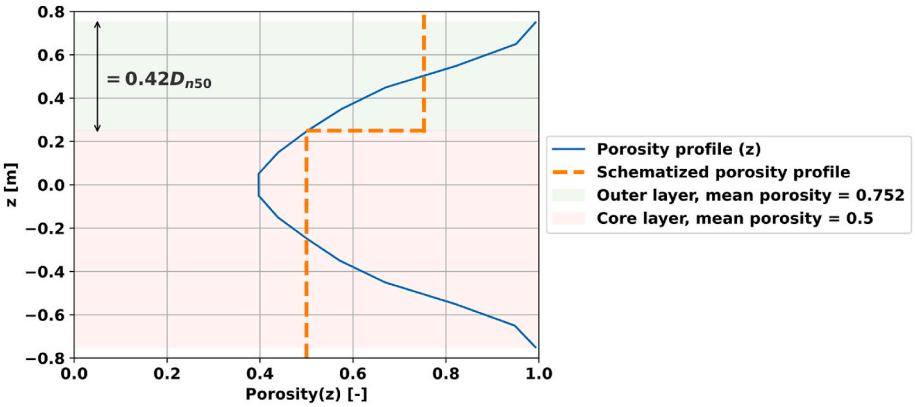

Fig. 4. Porosity distribution for one layer of randomly placed Cubipod armor with layer formation ($a/D_{n50} = 1.58$ and $b/D_{n50} = 1.27$). The outer layer has a layer thickness of 0.42 $D_{n50} = 1.8$ cm and a porosity of 75.2%, whereas the core has a porosity of 50%.

The outer layer is defined as the layer between the intersection of the porosity distribution with the mean porosity (50%) and the outside of the concrete element (highlighted in light green in Fig. 4). The mean porosity of this layer was derived by taking the mean value of the porosity distribution of the outer layer, which was found to be 75.2% corresponding to an outer layer thickness of 0.42 D_{n50}.

2.4.2.2. HLCS closure coefficients. The calibration case should be as close as possible to the intended use of the model. This study aims to describe the porous behavior of an HLCS with a crest freeboard of approximately zero for a constant set of boundary conditions. Hence, the values of the wave characteristics (i.e., significant incident wave height, peak wave period, and wave transmission coefficient) were used, as presented in Table 1. Furthermore, the time-resolved hydraulic boundary conditions of the physical modeling experiment were unknown. The hydraulic boundary conditions corresponding to the incoming wave characteristics at the sloping foreshore (wave gauge 2; Fig. 1) were used for the offshore boundary of the OceanWaves3D model coupled with the OpenFOAM model. The calibration was performed on the wave transmission coefficient by comparing the measured experimental wave transmission coefficient ($K_{t,extracted}$; of the calibration case) and the predicted wave transmission coefficient by OpenFOAM ($K_{t,OpenFOAM}$) for different combinations of closure coefficient values ($500 < \alpha < 2500$ and $0.2 < \beta < 6$). The results were only sensitive to different values of β. The best agreement between $K_{t,extracted}$ and $K_{t,OpenFOAM}$ was noted at $\alpha = 500$ and $\beta = 1.0$ with uncertainty of only 0.7%.

The OpenFOAM model was then validated to predict the wave transmission associated with the HLCS using calibrated porous media resistance parameters for different values of $H_{s,i}$, $T_{p,i}$, and R_c as reported in the physical modeling experiment by Medina et al. (2019). For different hydraulic boundary conditions, model runs with and without the HLCS were conducted to avoid the need for a wave-reflection procedure, as previously described in the calibration methodology. Hence, the validated range of model applicability is $-0.1 < R_c/H_{s,i} < 0.38$. It is noted that the OpenFOAM model underpredicted the wave transmission for all of the performed numerical experiments with a mean of 6.6%. The lowest error of 2.6% was noted for the HLCS with a crest level around the SWL ($R_c \approx 0$). This is logical, because the numerical model was calibrated for such a condition. For more details on the calibration and validation procedures of the HLCS hydrodynamic behavior, please refer to Jonker (2020).

3. Results and discussion

3.1. Design sensitivity analysis

In this section, the OpenFOAM-validated model is used to extend the limited available knowledge on the design considerations of an HLCS made of Cubipod concrete elements to reduce overtopping at a seawall. For the basic configuration, the effects of changing a single parameter of the main geometric layout (h_c. B, and L_B, see Fig. 5) on K_t, mean water level setup near the seawall ($\overline{\eta}_{seawall}$), and q, were analyzed. When

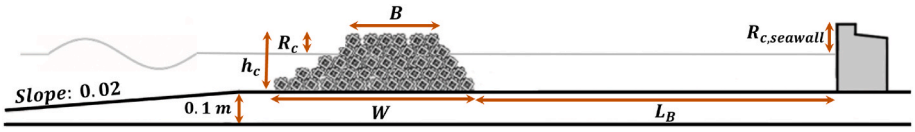

Fig. 5. Outline of the geometrical parameters investigated in this design sensitivity analysis study.

varying L_B, the HLCS was maintained at the same location, whereas the seawall moved landward. When varying B, the width increased landward, as did the location of the seawall, to keep L_B constant. When varying h_c, the number of Cubipod layers was varied (by one layer) as well as W to maintain a constant B. Owing to the high reflectivity of the seawall, the wave field inside the basin (the lee side of the HLCS) consisted of waves traveling landward and seaward. Only landward waves were considered to obtain K_t. To obtain transmitted wave signals, a wave reflection procedure based on Zelt and Skjelbreia (1993) was used with gauges 5–7. The $\overline{\eta}_{seawall}$ is evaluated directly adjacent to the seawall and is defined as the difference between the mean instant water level and the still water level in the flume. The overtopping discharge was determined by integrating the water flowing through the plane extending above the front face of the seawall. The basic configuration is described by a relative crest-free board ($R_c/H_{s,i}$), relative crest width ($B/H_{s,i}$), and relative basin length (L_B/L_p) of 0, 3.0, and 1.2, respectively (Table 2). Afterward, these parameters were independently varied according to the ranges $-0.4 < R_c/H_{s,i} < 0.8$, $1.5 < B/H_{s,i} < 15$, and $0.5 < L_B/L_p < 1.8$. A high level of nonlinearity was noted between the parameters without a simple trend. Hence, the effects of changing these parameters are thoroughly investigated in the following subsections.

3.1.1. Effect of changing the crest freeboard

$R_c/H_{s,i}$ was varied between −0.4 and 0.8, whereas $B/H_{s,i}$ and L_B/L_p were kept equal to the values of the basic configuration, as given in Table 2. Fig. 6a shows the wave transmission over the HLCS (blue dotted line) and the mean overtopping discharge over the vertical seawall (green dotted line) corresponding to different crest freeboards. By increasing the crest height, a strong initial decay in the mean overtopping discharge was observed. This behavior is closely related to the trend of the wave transmission coefficient, indicating that wave transmission strongly influences the mean overtopping discharge. In Fig. 6a, the wave transmission coefficients obtained in this study are compared with those of Medina et al. (2019) wave transmission coefficients (black dotted line). A similar relationship is observed between the two results. Notably, the difference in magnitude is due to the smaller crest width of $B/H_{s,i} = 1.0$, used by Medina et al. (2019), compared with the larger crest width of $B/H_{s,i} = 3.0$, used in the OpenFOAM model. A slight increase in wave transmission with freeboard was noted with the emergent HLCS ($R_c > 0$), whereas a continuous reduction was expected for a conventional rubble-mound LCS. It is likely that this effect is mainly caused by the higher porosity of the HCLS in combination with the larger element sizes compared to the conventional rubble-mound LCS. Hence, wave energy can be transported through the larger pores of the HLCS with less energy dissipation, and therefore, increased wave transmission. Moreover, higher porosity affects wave shoaling and breaking, and lower wave energy dissipation is expected at the crest of the HLCS (Hattori and Sakai, 1994).

In this study, a small increase in the wave transmission coefficients was observed for emergent HLCS ($R_c > 0$), whereas Medina et al. (2019) observed a more constant trend for emergent HLCS ($R_c > 0$). This difference could be caused by uncertainties related to the influence of the water level setup behind the HLCS, wave reflection caused by the seawall, or the accuracy of the physical modeling measurements (e.g., the wave reflection procedure and duration of the measurements). Fig. 6b shows the mean water level setup near the seawall (orange dotted line) and the mean overtopping discharge for different crest heights of the HLCS. As the crest height increases, the water level setup also increases until it reaches its maximum around slightly emergent structures ($0 \leq R_c/H_{si} \leq 0.4$). Subsequently, the mean water level decreased for the emergent structures ($R_c > 0.4$). This trend in the water level setup was similar to the results obtained by Loveless et al. (1998), who also found that the maximum water level setup to occur when the crest was around the SWL. Here the influx of water due to overtopping increases, but no large backflow over the LCS has occurred yet. In the present study, the exact maximum water level setup cannot be extracted due to the lack of additional data points; however, it is expected to have the maximum water level setup within this region of slightly emergent structures ($0 \leq R_c/H_{si} \leq 0.4$).

Table 2
Values of the parameters used to perform the design sensitivity analysis.

Cases	Value of Parameters
Basic configuration	$R_c/H_{s,i} = 0$, $B/H_{s,i} = 3.0$, $L_B/L_p = 1.2$
Changing $R_c/H_{s,i}$	$-0.4 < R_c/H_{s,i} < 0.8$, $B/H_{s,i} = 3.0$, $L_B/L_p = 1.2$
Changing $B/H_{s,i}$	$R_c/H_{s,i} = 0$, $1.5 < B/H_{s,i} < 15$, $L_B/L_p = 1.2$
Changing L_B/L_p	$R_c/H_{s,i} = 0$, $B/H_{s,i} = 3.0$, $0.5 < L_B/L_p < 1.8$

3.1.2. Effect of changing the crest width

Next, $B/H_{s,i}$ was varied between 1.5 and 1, whereas $R_c/H_{s,i}$ and L_B/L_p were maintained equal to the values of the basic configuration, as listed in Table 2. Fig. 7a shows the wave transmission coefficients (blue dotted line) and mean overtopping discharges (green dotted line) for different crest widths of the HLCS. By increasing the crest width, a similar exponential-like decay was noted in both the wave transmission coefficients and mean overtopping discharge. This behavior indicates that the wave transmission over the reef strongly influences the mean overtopping discharge at the vertical seawall. The amount of wave transmission was influenced by the amount of wave energy dissipation owing to the two dissipation mechanisms and reflection. The first dissipation mechanism involves wave breaking at the crest of a structure, which causes turbulence and energy dissipation. The second dissipation mechanism is energy dissipation via porous flow. The concept of breaker travel distance was used to roughly estimate the most effective crest width related to energy dissipation by wave breaking (Shore Protection Manual, 1984):

$$x_p = (4.0 - 9.25\ m) \bullet H_b, \tag{13}$$

where x_p is the breaker travel distance; m is the foreshore slope (0.02); and H_b is the breaker wave height. For the given boundary conditions, a crest width of $B/H_{s,i} = 4.4$ was obtained. Therefore, for smaller crest widths ($B/H_{s,i} \lesssim 4.5$), the reduction in the wave transmission coefficient was primarily related to the enhanced wave breaking on the crest of the HLCS, whereas for larger crest widths ($B/H_{s,i} > 4.5$), it was primarily related to the enhanced porous flow resistance as it traveled through the structure. In Fig. 7a, a gradual decrease in the effectiveness of wider crests is noted for $B/H_{s,i} \gtrsim 4.5$ as past this benchmark, most of the wave's energy would dissipate due to the enhanced porous flow resistance; hence, smaller differences would be noted in the values of wave transmission. Fig. 7b presents the mean water level setup near the seawall (orange dotted line) and the mean overtopping discharge. For wider crests ($B/H_{s,i} \gtrsim 4.5$), increased porous water resistance is expected; hence, most of the wave energy dissipates. Therefore, the water level setup remained constant past this benchmark with minor differences. Moreover, the behavior of the water level setup inside the basin has little

a)

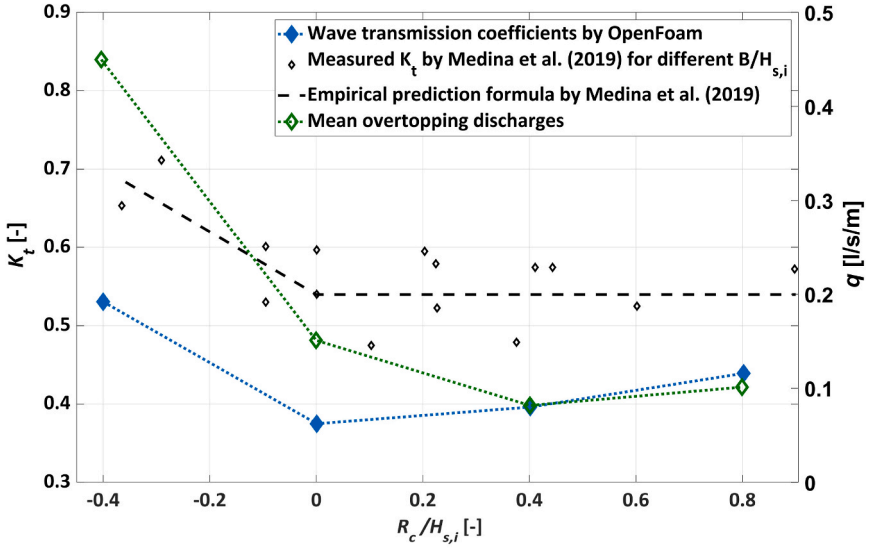

b)

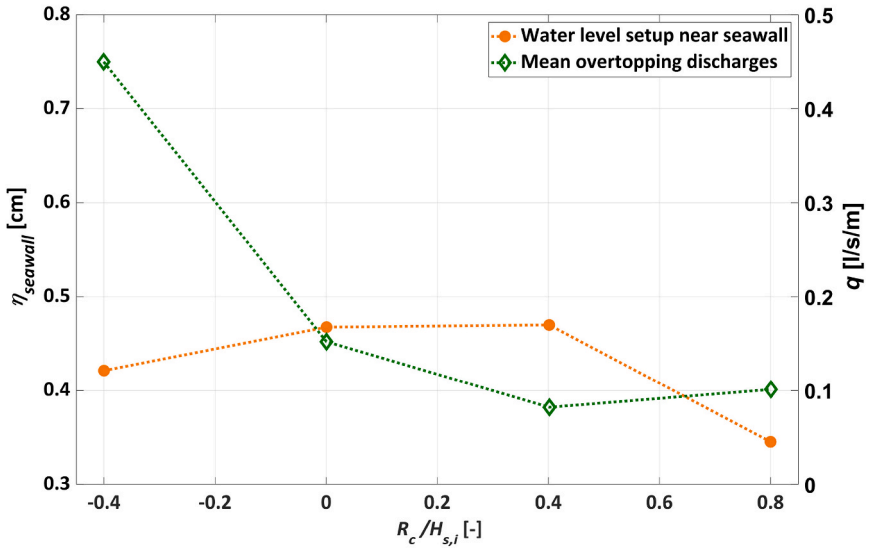

Fig. 6. Effect of changing the relative crest freeboard for $B/H_{s,i} = 3.0$ (note that Medina et al. (2019) used different $B/H_{s,i}$ value of 1.0) and $L_B/\ L_p$ of 1.2 on a) wave transmission coefficient and the predicted mean overtopping discharge and b) water level setup and the predicted mean overtopping discharge.

effect on the mean overtopping discharge compared with the dominant influence of wave transmission, as observed in Fig. 7a.

To further understand the effect of the HLCS on wave transmission, the wave transmission coefficients obtained from the OpenFOAM model (blue dots) for the HLCS were compared with the data used by Van der Meer et al. (2005) to obtain empirical prediction guidelines for a conventional rubble-mound LCS with zero freeboards (Fig. 8). The empirical prediction guidelines (Eqs. Fourteen and 15) by Van der Meer et al. (2005) were based on an extensive experimental investigation of conventional rubble-mound LCS with different crest widths under non-breaking, breaking, and broken waves.

$$K_t = -0.4\frac{R_c}{H_{s,i}} + 0.64\left(\frac{B}{H_{s,i}}\right)^{-0.31}\left(1 - e^{-0.5\xi}\right), \text{for } \frac{B}{H_{s,i}} < 8 \tag{14}$$

$$K_t = -0.35\frac{R_c}{H_{s,i}} + 0.51\left(\frac{B}{H_{s,i}}\right)^{-0.65}\left(1 - e^{-0.41\xi}\right), \text{for } 12 > \frac{B}{H_{s,i}} > 50. \tag{15}$$

Fig. 8 shows a similar trend in wave transmission between the HLCS and conventional rubble mound LCS. Furthermore, the data for the HLCS fit well with the empirical prediction formulas and were located within the bandwidth of the scatter of the underlying data used by Van der Meer et al. (2005) for the conventional rubble-mound LCS. However, for a crest width of $B/H_{s,i} \approx 10$, the Van der Meer et al. (2005) equations provide an ambiguous answer and very different results. Moreover, these equations do not include the HLCS (the main focus of this study).

Therefore, a fitted curve equation was explicitly derived for the HLCS based on the OpenFOAM model as follows:

$$K_t = 0.59\left(\frac{B}{H_{s,i}}\right)^{-0.496} \tag{16}$$

The fitted curve fits all data points well. This equation can be used for the initial assessment of the wave transmission in an HLCS. This equation, in combination with that of Medina et al. (2019), describes the

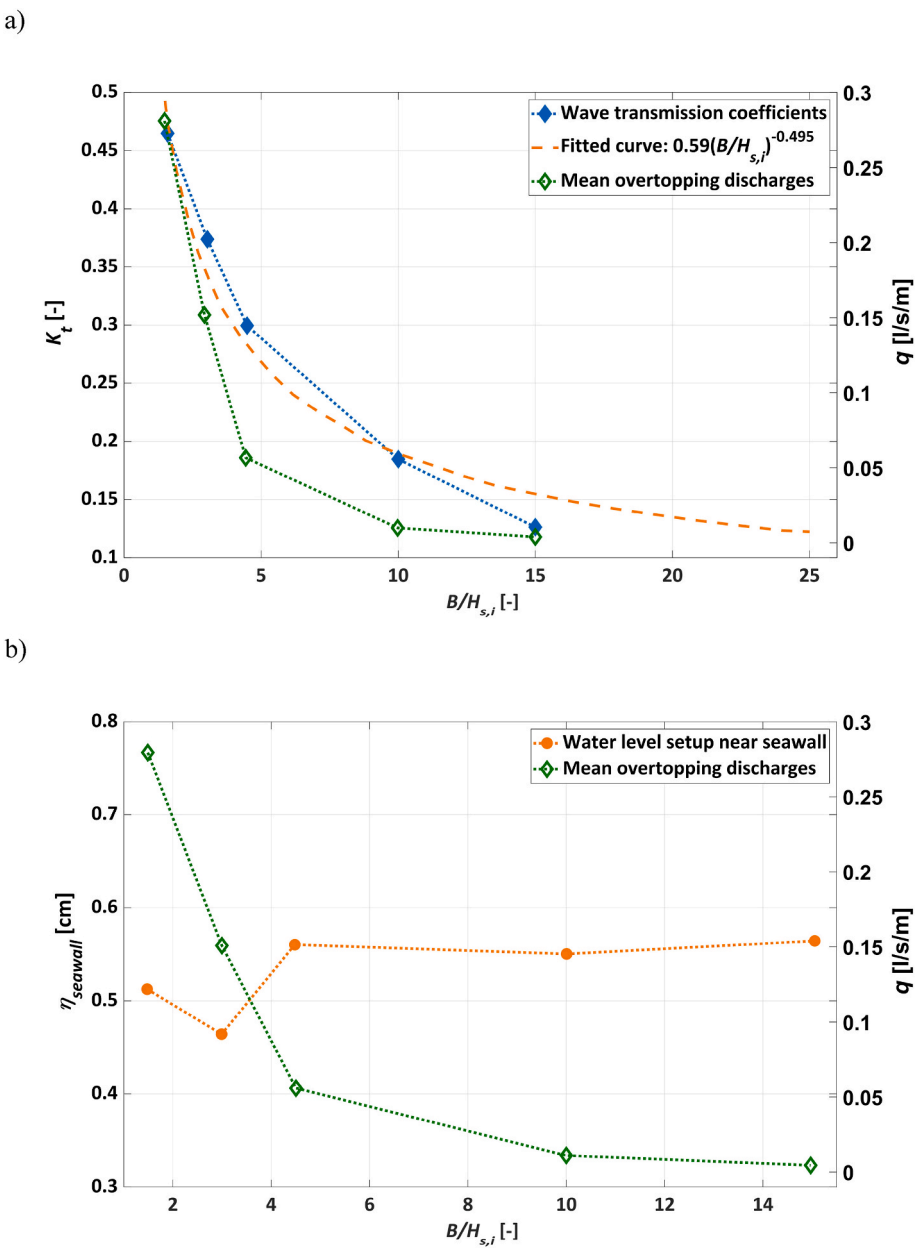

Fig. 7. Effect of changing the relative crest width for $R_c/H_{s,i} = 0$ and L_B/L_p of 1.2 on a) wave transmission coefficient and the predicted mean overtopping discharge and b) water level setup and the predicted mean overtopping discharge.

effect of relative crest height on wave transmission for HLCS and provides a good estimation of the hydraulic performance of wave transmission for these structures. The effects of the relative crest height and crest width can therefore be included in the transmission prediction of the HLCS, as in the equations of Van der Meer et al. (2005).

Hence, it is concluded that the newly fitted equation is best used for the initial evaluation of the effect of the HLCS crest width on wave transmission, particularly around $B/H_{s,i} = 10$.

3.1.3. *Effect of changing the basin length*

The effect of changing L_B was investigated according to the procedure described in Section 3.1. Therefore, L_B/L_p varied between 0.5 and 1.8, whereas $R_c/H_{s,i}$ and $B/H_{s,i}$ were kept equal to the values of the basic case, as listed in Table 2. The wave transmission coefficients (blue dotted line) and mean overtopping discharges (green dotted line) corresponding to different basin lengths are shown in Fig. 9a. An exponential-like decay was observed in the mean overtopping discharge as the basin length increased. However, the wave transmission coefficient exhibited a constant trend because no changes were made to the HLCS cross-section. The water level setup (orange dotted line) and mean overtopping discharge for different basin lengths are shown in Fig. 9b. The mean water level near the seawall increased as the basin length increased, whereas the mean overtopping discharge decayed exponentially. Visual inspection of the simulations showed that the breaking waves over the HLCS for smaller basin lengths created hydraulic bores that traveled above the SWL and caused extensive overtopping of the seawall. These traveling bores lose energy owing to the turbulence during propagation. This explains why less overtopping is observed for larger basin lengths. Furthermore, smaller basins have less storage volume, which causes a faster increase in the water level inside the basin as the wave groups enter (i.e., larger water-level gradients). Hence, smaller waves at the end of a wave group can surpass the seawall. These waves were unable to surpass the seawall in larger basins because of the larger storage volume and therefore lower water levels during the wave group

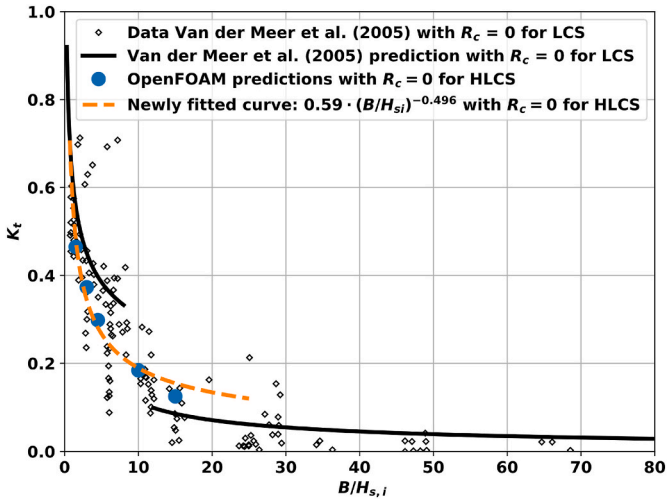

Fig. 8. Effect of changing the HLCS crest width on wave transmission as predicted by OpenFOAM (blue dots), including a fitted curve (orange dashed line), compared to the empirical prediction guideline by Van der Meer et al. (2005) for conventional rubble-mound LCS (black solid line). Data are adopted from Van der Meer et al. (2005).

propagation inside the basin. It is also noted in Fig. 9b that the faster increase and decrease in the water level inside the smaller basins does not influence the mean water level setup near the seawall.

A continuous (partial) reflection between the HLCS and the seawall can create standing waves, which cause seiching-resonance if the natural frequency of the wave is equal to the eigenfrequency of the basin. These low-frequency waves can also enhance sloshing in the basin, thereby increasing the mean overtopping discharge at higher water levels. Multiple simulations were performed with different basin lengths to understand the effects of the seiching-resonance within the basin. This was achieved by comparing raw wave spectra near the seawall for each tested basin length. Furthermore, the theoretical resonance frequencies for a closed basin were determined and the raw wave spectra near the seawall were compared for different basin lengths. For basin lengths equal to 0.5, 1.0, and 1.5 L_B/L_p, more overtopping is expected owing to the seiching-resonance. A match was noted between the theoretical resonance frequencies and energy peaks of these wave spectra. Additionally, some basins with lengths equal to the theoretical resonance basin lengths had slightly larger mean overtopping discharges. However, the increase in overtopping was not significant. For more details on the effect of the seiching-resonance on overtopping at the seawall, please refer to Jonker (2020).

3.2. Design recommendations

Based on the design sensitivity analysis performed in the previous section, design recommendations for the geometric parameters are provided in this section. The effects of changing the relative freeboard, relative crest width, and relative basin length on the wave transmission coefficients and mean overtopping discharge at the seawall are presented in Fig. 6a, 7a and 9a, respectively. For all tested geometrical parameters, it was noted that increasing them caused an exponential-like decay in the mean overtopping discharge. These results were previously discussed in detail; however, we revisited them in this section to obtain the optimal geometrical parameters for the HLCS. The optimal design parameters were selected based on the maximum effectiveness of the parameters in reducing the mean overtopping discharge, where the largest gradient in overtopping was noted. By selecting smaller values for these parameters, greater overtopping is expected at the seawall. In contrast, larger values are expected to reduce overtopping and increase construction costs. Therefore, engineers are responsible for designing according to the site conditions, performance requirements, and available budgets.

By examining Fig. 6a, 7a and 9a, the largest gradient in the mean overtopping discharge is noted at $R_c/H_{s,i} \approx 0$, $B/H_{s,i} \approx 4.5$, and $L_B/L_p \approx 1.2$. These values are dependent on the number of data points used. Ideally, it is preferred to have continuous data points for all different configurations. The number of available data points is, however, limited by the large computational time of the simulations, which were not available to the authors. The exact value of the largest gradient may vary around the presented value (e.g., if $B/H_{s,i} = 6$ is available, the largest gradient may be a little different than the currently obtained one). However, it is expected that the presented values give a good estimation for design purposes. Hence, $R_c \approx 0$ is recommended for the design of HLCS, especially that increasing the crest height would increase the construction cost. This is because the base width increases as the height of the structure increases. The effective crest width corresponding to the maximum gradient in the mean overtopping discharge was approximately equal to the crest width at which the maximum wave energy dissipation by wave breaking was noted. It was found that the effective width could be estimated using the concept of the breaker travel distance. This concept is expected to be valid under different wave and boundary conditions. Based on OpenFOAM simulations, the effect of the relative crest width on the wave transmission for the initial estimation can be best described using Eq. (16). For $L_B/L_p < 1.2$, it was noted that the wave breaking on top of the HLCS caused the propagation of hydraulic bores and extensive overtopping at the seawall. Hence, a basin length of roughly $L_B/L_p \approx 1.2$ is recommended, at which the maximum gradient in the mean overtopping discharged was noted. For a beach with a steep slope, it is more economical to increase the crest height or width and decrease the basin length to minimize overtopping at the seawall.

In this study, it was noted that overtopping was mainly dominated by wave transmission (influenced by the width and height of the structure) and bore dissipation behind the HLCS (influenced by the basin length) and was less influenced by the water level setup and seiching-resonance. Hence, an additional assessment was performed without a CFD model to predict the overtopping discharge based on wave transmission only and without the water level setup effect or any additional hydrodynamics associated with the difference in basin length (e.g., low-frequency wave motion and broken wave propagation). A comparison was made between the overtopping discharges estimated using EurOtop guidelines based on wave transmission only (keeping the water level in the basin equal to the offshore value) and those obtained using the OpenFOAM model. A mean underestimation of 69% was noted. Hence, the effects of the water level setup, bore propagation, and seiching-resonance were not negligible. Advanced CFD models (e.g., OpenFOAM) or physical modeling are important for evaluating overtopping, particularly for systems with complex hydrodynamics influenced by dissipating bores and seiching-resonance inside the basin.

4. Conclusions, limitations, and recommendations

4.1. Main conclusions

The main geometric parameters that significantly influenced the hydrodynamic performance of the HLCS composed of Cubipod concrete elements and overtopping events were R_c, B, and L_B. OpenFOAM can be used to numerically model the hydrodynamic behavior of porous structures using the Van Gent (1995) parameterization of the extended Darcy–Forchheimer equation, similar to the VARANS equations. The best agreement between the modeled and experimental transmission coefficients is found at $\alpha = 500$ and $\beta = 1.0$ in combination with two numerical layers with a core porosity of 50% and an outer layer (0.42 D_{n50}) porosity of 75.2%.

By assessing overtopping for different HLCS crest heights and widths,

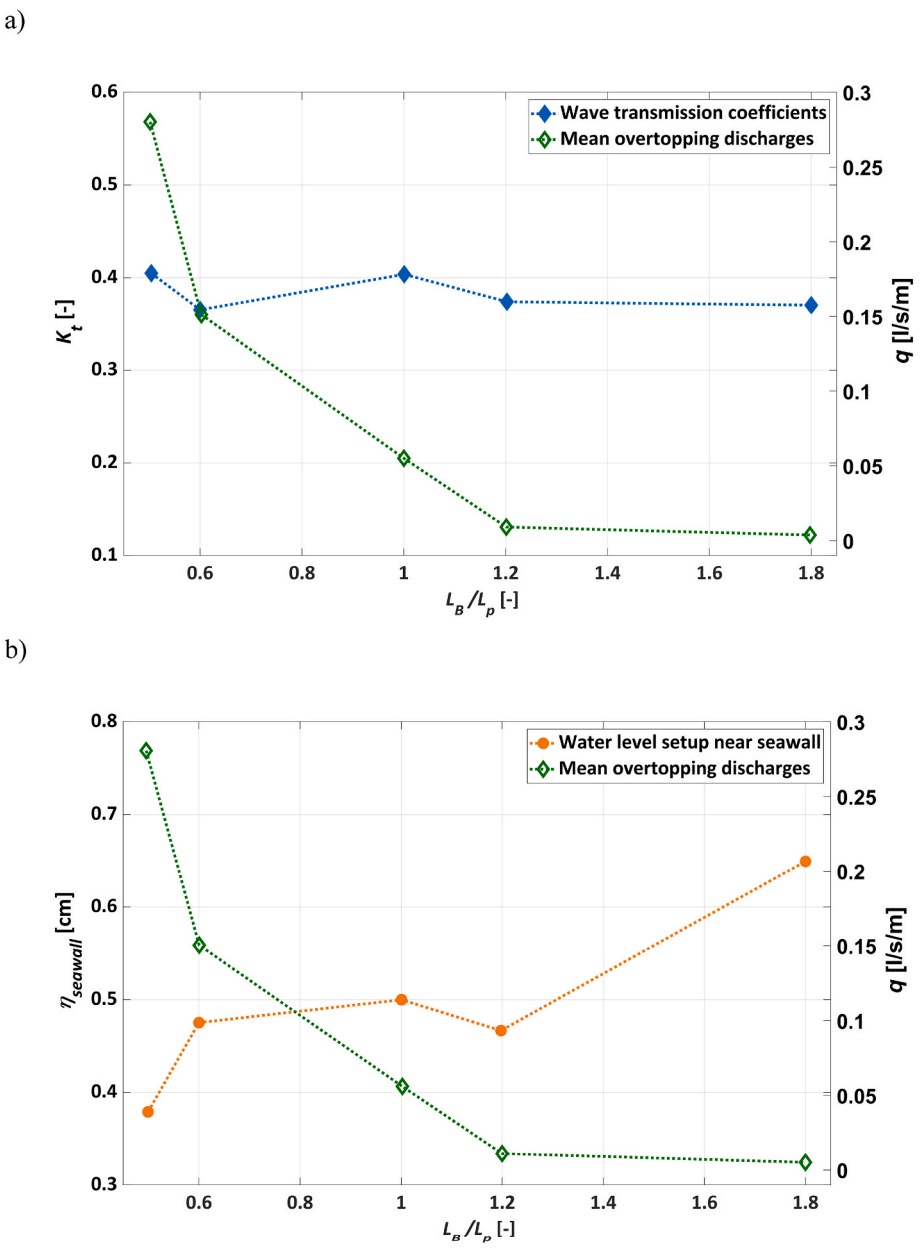

Fig. 9. Effect of changing the relative basin length for $R_c/H_{s,i} = 0$ and $B/H_{s,i} = 3.0$ on: a) wave transmission coefficient and the mean overtopping discharge and b) water level setup and the mean overtopping discharge.

it was found that the mean overtopping discharge was dominated by wave transmission and broken bore dissipation and was less influenced by the water level setup and seiching-resonance. The broken wave propagation (i.e., hydraulic bores) due to waves breaking over the HLCS crest significantly impacts the mean overtopping discharge. Notably, these hydraulic bores fade at larger basin lengths.

An exponential-like decay is noted in the overtopping discharge when the values of all the tested geometrical parameters (R_c, B, and L_B). The most influential parameter for overtopping was found to be R_c. The largest gradient in the mean overtopping discharge is noted at $R_c/\ H_{s,i} \approx 0$, $B/H_{s,i} \approx 4.5$, and $L_B/L_p \approx 1.2$. Hence, it is recommended to construct an HLCS using these values for the geometrical parameters. For comparable hydraulic boundary conditions (i.e. the same order of H_s, H_s/h, h/L_p) with similar homogeneous low-crested structures (i.e. $R_c/H_{s,i} \approx 0$) in front of vertical or sloping seawalls, it is expected that this OpenFOAM model can be used without further calibration.

4.2. Limitations and recommendations

This subsection discusses the study limitations and proposed recommendations for future studies. The influence of changing the geometrical parameters in this study was assessed independently by varying only one parameter per simulation using the basic configuration as a starting point. The basic configuration is a single predefined set of values for the geometrical layout parameters related to the conducted physical model experiments with the corresponding geometry of the HLCS and flume layout dimensions. Because the geometrical layout parameters are not varied simultaneously, the results may have a dependency on the chosen basic configuration. The authors expect similar results of the main geometrical parameters using a different basic configuration. However, to avoid the uncertainty in the selected basic configuration, it is recommended to investigate the dependency of the geometrical parameters on each other in a more comprehensive test matrix as it may provide additional information that can be used for

design considerations and reduces the impact of the adopted basic configuration.

Additionally, to gain more insight into the hydrodynamic performance of the HLCS itself, it is recommended that the wave reflection and energy dissipation within the structure be investigated in relation to the adopted Darcy–Forchheimer parameters. Moreover, in this study, it was found that changing L_B had a major influence on the overtopping discharge at $R_c/H_{s,i} \approx 0$, likely due to hydraulic bores. Hence, it would be interesting to: a) assess the effect of changing this parameter when the HLCS is submerged or emerged, and b) investigate and assess the influence of bore propagation. The decay of waves in the basin between the seawall and HLCS reef-type structure is driven by turbulence, which is not yet perfectly included in OpenFOAM. To validate the numerical model and initial prediction formula for a larger range of input parameters, a thorough physical modeling investigation of a wide range of crest widths for the HLCS is recommended. The equation obtained to describe the effect of the relative crest width of the HLCS on wave transmission is not a general equation because it is based on only one wave condition (H_s, T_p). Hence, it is recommended that this formula be generalized for different wave conditions. Furthermore, the combined effect of the relative crest height and crest width on wave transmission, following the work of Medina et al. (2019) and this study was analyzed.

CRediT authorship contribution statement

R.G. Jonker: Data curation, Writing – review & editing, Writing – original draft, Visualization, Validation, Software, Project administration, Methodology, Investigation, Formal analysis, Conceptualization. **Ahmad AlYousif:** Data curation, Writing – review & editing, Writing – original draft, Visualization, Validation, Supervision, Investigation, Formal analysis. **B. Hofland:** Writing – review & editing, Supervision, Methodology, Conceptualization. **Alessandro Antonini:** Supervision, Methodology, Conceptualization. **Arthur Zoon:** Supervision, Resources, Methodology, Conceptualization. **Gregory Smith:** Supervision, Resources, Conceptualization.

Declaration of competing interest

The authors declare that they have no known competing financial interests or personal relationships that could have appeared to influence the work reported in this paper.

Data availability

Data will be made available on request.

Acknowledgments

The authors thank Van Oord for allowing them to implement some non-open-source tools and processing utilities in the numerical framework, which were developed as part of the JIP Coastal FOAM Program to validate and expand the usage of OpenFOAM as a design tool for different coastal engineering applications.

Nomenclature

α and β	Closure coefficients
a_p and b_b	Drag force resistance coefficients
B	Crest width
$B/H_{s,i}$	Relative crest width
C_{max}	Maximum Courant number
Cov	Co-variance between the two random time signals (X_1 and X_2)
c_p	Mass coefficient
χ	Weighting factor
D_{n50}	Nominal median diameter
F	Indicator field function
$\boldsymbol{F}_p$	Vector of flow resistance
f	Set of faces in the mean overtopping discharge equation
$\boldsymbol{g}$	Vector of gravitational acceleration
γ_p	Empirical coefficient
HLCS	Homogeneous low-crested structure
H_b	Breaker wave height
H_{m_0}	Significant wave height using spectral analysis ($H_{m_0} = 4\sqrt{m_0}$)
H_s	Offshore boundary wave height
$H_{s,i}$	Incoming measured significant wave height at WG02
$H_{s,t}$	Transmitted significant wave height
h_0	Offshore water depth at WG00
h	Water depth in the basin at WG05
h_c	Crest height
KC	Keulegan-Carpenter number
K_t	Wave transmission coefficient
$K_{t,extracted}$	Measured experimental wave transmission coefficient
$K_{t,OpenFOAM}$	Predicted wave transmission coefficient by the OpenFOAM
LCS	Low-crested structure
L_B	Basin length
L_B/L_p	Relative basin length based on peak wavelength in the basin
m	Foreshore slope
μ	Dynamic viscosity
N	Number of observations within the signal
n_p	Porosity

$n_{p,core}$	mean porosity of the core
$n_{p,outer}$	mean porosity of the outer layer
∇	Gradient operator
ν	Kinematic viscosity
PCC	Pearson correlation coefficient
p	Total pressure
p^*	Excess pressure
φ_F	The flux of fluid across a face multiplied with the indicator function F
$\varphi_{computed}$	Numerical solution
φ_{target}	Target solution
q	Mean overtopping discharge
RMSE	Root mean squared error
RANS	Reynolds averaged Navier-Stokes
R_c	HLCS crest freeboard
$R_c/H_{s,i}$	HLCS relative crest freeboard
$R_{c,seawall}$	Seawall crest freeboard
Re_p	pore Reynolds number
ρ	Fluid Density
ρ_c	Mass density
SWL	Still water level
s_f	Non-unit normal vector to the face
$s_{m-1,0}$	Wave steepness
σ	The standard deviation of each random time signal
$T_{m-1,0}$	Spectral wave period
t	Time
$\boldsymbol{u}$	Filter velocity in Cartesian coordinates
$\boldsymbol{u}^T$	Transpose of $\boldsymbol{u}$
$\boldsymbol{u_r}$	Relative velocity
$\langle\overline{u}\rangle$	Averaged flow velocity per time step per control volume (computational cell)
VARANS	Volume averaged RANS
VOF	Volume of fluid
W	Structure's base width
$\boldsymbol{x}$	Cartesian coordinate vector
x_p	Breaker travel distance
$\widehat{y}_i$	The predicted value in RMSE
y_i	The observed value in RMSE

References

AlYousif, A., AlKhaldi, M.S., Al-Amer, F., Neelamani, S., 2021. Hydrodynamic characteristics of a vertical wall with an immersed horizontal plate subjected to regular and random waves. Ocean. Eng. 236, 109489 https://doi.org/10.1016/j.oceaneng.2021.109489.

AlYousif, A., AlKhaldi, M.S., Al-Amer, F., Neelamani, S., 2022. Wave action on a vertical wall with a submerged horizontal plate: analysis of phase variation of forces and probability of Exceedance. Int. J. Nav. Archit. Ocean Eng. 14, 100429. https://doi.org/10.1016/j.ijnaoe.2021.100429.

Berberović, E., Van Hinsberg, N.P., Jakirlić, S., Roisman, I.V., Tropea, C., 2009. Drop impact onto a liquid layer of finite thickness: dynamics of the cavity evolution. Phys. Rev. E - Stat. Nonlinear Soft Matter Phys. https://doi.org/10.1103/PhysRevE.79.036306.

Briganti, R., Van Meer, J.D., Buccino, M., Calabrese, M., 2003. Wave transmission behind low-crested structures. Coast. Struct. 2003 - Proc. of Conf. 580–592. https://doi.org/10.1061/40733(147)4.

Buccino, M., Calabrese, M., 2007. Conceptual approach for prediction of wave transmission at low-crested breakwaters. J. Waterw. Port, Coast. Ocean Eng. 133 (3), 213–224. https://doi.org/10.1061/(ASCE)0733-950X, 2007)133:3(21.

Calabrese, M., Vicinanza, D., Buccino, M., 2003. 2D Wave Set up behind Low Crested and Submerged Breakwaters. Proc. Int. Offshore Polar Eng. Conf, Honolulu, HI, USA.

Calabrese, M., Vicinanza, D., Buccino, M., 2008. 2D Wave setup behind submerged breakwaters. Ocean Eng. 35 (10), 1015–1028. https://doi.org/10.1016/j.oceaneng.2008.03.005.

del Jesus, M., Lara, J.L., Losada, I.J., 2012. Three-dimensional interaction of waves and porous coastal structures. Part I: Numerical model formulation. Coast. Eng. 64, 57–72. https://doi.org/10.1016/j.coastaleng.2012.01.008.

Diskin, M., Vajda, M., Amir, I., 1970. Piling-up behind low and submerged permeable breakwaters. J. Waterw. Harb. Coast. Eng. Div. https://doi.org/10.1061/AWHCAR.0000022.

D'Angremond, K., Van Der Meer, J.W., De Jong, R.J., 1996. Wave transmission at low-crested structures. Proc. Coast. Eng. Conf. https://doi.org/10.9753/icce.v25.%25pdelJesus.

Engsig-Karup, A.P., Bingham, H.B., Lindberg, O., 2009. An efficient flexible-order model for 3D nonlinear water waves. J. Comput. Phys. https://doi.org/10.1016/j.jcp.2008.11.028.

Hattori, M., Sakai, H., 1994. Wave breaking over permeable submerged breakwaters. Coast. Eng. 24 https://doi.org/10.1061/9780784400890.081.

Higuera, P., Lara, J.L., Losada, I.J., 2014a. Three-dimensional interaction of waves and porous coastal structures using OpenFOAM®. Part I: formulation and validation. Coast. Eng. 83, 243–258. https://doi.org/10.1016/j.coastaleng.2013.08.010.

Higuera, P., Lara, J.L., Losada, I.J., 2014b. Three-dimensional interaction of waves and porous coastal structures using OpenFOAM®. Part II: application. Coast Eng. https://doi.org/10.1016/j.coastaleng.2013.08.010.

ITTC, 2011. ITTC-recommended procedures and guidelines: practical guidelines for ship CFD applications. Tech. Rep.

Jacobsen, N.G., Fuhrman, D.R., Fredsøe, J., 2012. A wave generation toolbox for the opensource CFD library: OpenFoam. Int. J. Numer. Methods Fluid. 70 (9), 1073–1088. https://doi.org/10.1002/fld.2726.

Jacobsen, N.G., Van Gent, M.R., Wolters, G., 2015. Numerical analysis of the interaction of irregular waves with two dimensional permeable coastal structures. Coast. Eng. 102, 13–29. https://doi.org/10.1016/j.coastaleng.2015.05.004.

Jacobsen, N.G., Van Gent, M.R., Fredsøe, J., 2017. Numerical modelling of the erosion and deposition of sand inside a filter layer. Coast. Eng. 120, 47–63. https://doi.org/10.1016/j.coastaleng.2016.09.003.

Jacobsen, N.G., Van Gent, M.R., Capel, A., Borsboom, M., 2018. Numerical prediction of integrated wave loads on crest walls on top of rubble mound structures. Coast. Eng. 142, 110–124. https://doi.org/10.1016/j.coastaleng.2018.10.004.

Jensen, B., Jacobsen, N.G., Christensen, E.D., 2014. Investigations on the porous media equations and resistance coefficients for coastal structures. Coast. Eng. 84, 56–72. https://doi.org/10.1016/j.coastaleng.2013.11.004.

Jonker, R.G., 2020. CFD study of the design sensitivities in the 2D geometrical layout using a detached homogeneous low-crested structure to reduce sea wall overtopping. MSc Thesis. Deft University of Technology.

Lamberti, A., Zanuttigh, B., 2004. Environmental Design of Low-Crested Coastal Defence Structures - (DELOS). European Conf. On Marine Science and Ocean Technology. Proc. of the EurOCEAN 2004, Galway, Ireland.

Longuet-Higgins, M., 1967. On the wave induced difference in mean sea level between two sides of a submerged breakwater. J. Mar. Res. 25 (2), 148–152. https://elischolar.library.yale.edu/journal_of_marine_research/1093.

Losada, I.J., Lara, J.L., del Jesus, M., 2016. Modeling the interaction of water waves with porous coastal structures. J. Waterw. Port, Coast. Ocean Eng. https://doi.org/10.1061/(ASCE)WW.1943-5460.000036.

Loveless, J.H., Debski, D., Macleod, A.B., 1998. Sea level set-up behind detached breakwaters. 568–570. 26th Int. Conf. on Coast. Eng. https://doi.org/10.1061/9780784404119.124.

Manual, Rock, 2007. The Use of Rock in Hydraulic Engineering, second ed. CIRIA, CUR, CETMEF, Published by C683, CIRIA, London (ISBN 978-0-86017-683-1 and 5.

Medina, J., Gómez-Martín, M.E., Mares-Nasarre, P., Odériz, I., Mendoza, E., Silva, R., 2019. Hydraulic performance of homogeneous low-crested structures. Coast. Struct. https://doi.org/10.18451/978-3-939230-64-9_007, 2019.

Molines, J., Bayon, A., Gómez-Martín, M.E., Medina, J.R., 2019. Influence of parapets on wave overtopping on mound breakwaters with crown walls. Sustainability. https://doi.org/10.3390/su11247109.

Odériz, I., Mendoza, E., Silva, R., Medina, J.R., 2018. Stability and hydraulic performance of a homogeneous Cubipod low-crested mound breakwater. 7th Int. Conf. on Appl. of Phys. Model. in Coast. Port Eng. Sci (p. 8). Santander.

Paulsen, B.T., Bredmose, H., Bingham, H.B., 2014. An efficient domain decomposition strategy for wave loads on surface piercing circular cylinders. Coast Eng. 86, 57–76. https://doi.org/10.1016/j.coastaleng.2014.01.006.

Pilarczyk, K.W., 2003. Design of low-crested (submerged) structures – an overview. 6th Int. Conf. On Coastal and Port Engineering in Developing Countries. Colombo, Sri Lanka.

Roenby, J., Larsen, B.E., Bredmose, H., Jasak, H., 2017. A new volume-of-fluid method in open-foam. In: 7th Int. Conf. On Comput. Methods in Mar. Eng (Marine 2017), Nantes, France.

Romano, A., Bellotti, G., Briganti, R., Franco, L., 2015. Uncertainties in the physical modelling of the wave overtopping over a rubble mound breakwater: the role of the seeding number and of the test duration. Coast Eng. https://doi.org/10.1016/j.coastaleng.2015.05.005.

Seabrook, S.R., Hall, K.R., 1998. Wave transmission at submerged rubblemound breakwaters. Proc. Coast. Eng. Conf. https://doi.org/10.9753/icce.v26.%25p.

Shore Protection Manual, 1984. Department of the Army, Waterways Experiment Station, Corps of Engineers. Coastal Engineering Research Center. https://doi.org/10.5962/bhl.title.47830.

Van den Bos, J., Verhagen, H., 2017. Breakwater Design - Lecture Notes CIE5308. Retrieved from. http://resolver.tudelft.nl/uuid:312f5a93-5a0a-406e-b697-a2798c75e3b5.

Van der Meer, J., 1990. Data on wave transmission due to overtopping (Tech. Rep.). Delft Hydraulics.

Van der Meer, J., Daemen, I., 1994. Stability and wave transmission at low-crested rubble-mound structures. J. Waterw. Port. Coast. Ocean Eng. 120 (1) https://doi.org/10.1061/(ASCE)0733-950X, 1994)120:1(1.

Van der Meer, J.W., Briganti, R., Zanuttigh, B., Wang, B., 2005. Wave transmission and reflection at low-crested structures: design formulae, oblique wave attack and spectral change. Coast. Eng. 52 (10–11), 915–929. https://doi.org/10.1016/j.coastaleng.2005.09.005.

Van der Meer, J., Allsop, N., Bruce, T., De Rouck, J., Kortenhaus, A., Pullen, T., Schüttrumpf, H., Troch, P., Zanuttigh, B., 2018. EurOtop. Retrieved from. www.overtopping-manual.com.

Van Gent, M.R., 1995. Porous flow through rubble-mound material. J. Waterw. Port, Coast. Ocean Eng. 121 (3), 176–181. https://doi.org/10.1061/(ASCE)0733-950X, 1995)121:3(17.

Vijay, K.G., Neelamani, S., AlYousif, A., 2022b. Hydrodynamic analyses of multiple porous plates attached to the front of a vertical composite breakwater. Ocean Eng. 266, 112964. https://doi.org/10.1016/j.oceaneng.2022.112964.

Vijay, K.G., Neelamani, S., AlYousif, A., 2022a. Numerical analysis of the performance of a horizontal porous plate attached to the front of a vertical wall. Ocean Eng 255, 111420. https://doi.org/10.1016/j.oceaneng.2022.111420.

Zanuttigh, B., Martinelli, L., Lamberti, A., 2008. Wave overtopping and piling-up at permeable low crested structures. Coast. Eng. 55 (6), 484–498. https://doi.org/10.1016/j.coastaleng.2008.01.004.

Zelt, J.A., Skjelbreia, J.E., Wave Technologies, 1993. Estimating incident and reflected wave fields using an arbitrary number of wave gauges. Proc. Coast. Eng. Conf. https://doi.org/10.9753/icce.v23.%25p.